Applied Physics Letters

Elucidating gigahertz acoustic modulation of extraordinary optical transmission through a two-dimensional array of nano-holes

Cite as: Appl. Phys. Lett. **110**, 091910 (2017); https://doi.org/10.1063/1.4977430
Submitted: 23 November 2016 • Accepted: 12 February 2017 • Published Online: 02 March 2017

R. Ulbricht, H. Sakuma, Y. Imade, et al.

AIP Publishing

Elucidating gigahertz acoustic modulation of extraordinary optical transmission through a two-dimensional array of nano-holes

R. Ulbricht,[1] H. Sakuma,[1] Y. Imade,[1] P. H. Otsuka,[1] M. Tomoda,[1] O. Matsuda,[1] H. Kim,[2] G.-W. Park,[2] and O. B. Wright[1,a)]

[1]*Division of Applied Physics, Graduate School of Engineering, Hokkaido University, Sapporo 060-8628, Japan*

[2]*School of Mechanical Engineering, Korea University, 145 Anam-ro, Seongbuk-gu, Seoul 136-713, Korea*

(Received 23 November 2016; accepted 12 February 2017; published online 2 March 2017)

The ultrafast modulation of light transmitted by a metamaterial making up an extraordinary optical transmission geometry is investigated by means of optical pump-probe spectroscopy. Using a sample consisting of a lattice of square nano-holes in a gold film on a glass substrate, we monitor the high-frequency oscillations in the intensity of transmitted infrared light. A variety of gigahertz acoustic modes, involving the opening and shutting motion of the holes as well as the straining of the glass substrate below the holes, are revealed to be active in the optical modulation. Numerical simulations of the transient deformations and strain fields elucidate the nature of the vibrational modes contributing most strongly to the variations in optical transmission, and point to the hole-area modulation as the dominant effect. Potential applications include ultrafast acousto-optic modulators. *Published by AIP Publishing.* [http://dx.doi.org/10.1063/1.4977430]

Extraordinary transmission of light through small sub-wavelength-sized holes[1–5] has resulted in a great deal of research on this phenomenon over a wide frequency range. The ability to squeeze an electromagnetic wave through a hole much smaller than its wavelength in this way has led to several suggestions concerning the possibility of electrically modulating transmitted terahertz waves in metamaterials consisting of arrays of small holes.[6,7] Another possibility for modulating the transmitted electromagnetic waves is the use of acoustic vibrations. Because the light can be squeezed through tiny holes, a given acoustic displacement should therefore result in an enhanced transmission modulation in such geometries. Gigahertz acoustic waves have been suggested for this purpose: Guyader *et al.*[8] demonstrated the coherent control of surface-plasmon-polariton (SPP) mediated extraordinary optical transmission (EOT) through two-dimensional (2D) arrays of circular nano-holes in a gold film on a garnet substrate by GHz surface acoustic waves induced by a sequence of ultrashort laser pulses. In addition, Gerard *et al.*[9] made a numerical study of GHz optoacoustic modulation in a 1D nano-slit-array piezoelectric EOT structure, and Yang *et al.*[10] made a numerical and experimental study of the GHz acoustic modulation of the transmission of a 1D nano-slit-array gold structure. However, acoustic studies of 2D EOT structures lack quantitative analysis of the vibrational modes excited, so that no detailed information was obtained on how the light was modulated for this case. Using samples consisting of square lattices of square nano-holes in a gold film on glass, we report here on the modulation of the intensity transmission in a 2D EOT geometry by gigahertz vibrational modes using a combination of experiment, based on ultrafast optical pumping and probing, and numerical simulation, based on the calculation of transient deformations and strain fields, thereby elucidating the acoustic modulation mechanisms in EOT.

The sample consists of a glass substrate (Schott D263) of 1 mm thickness coated with a 40 nm polycrystalline gold film, in which regular square holes of side 250 nm and pitch of 710 nm were created in a square-lattice array, as shown by the scanning electron micrograph (SEM) in the inset of Fig. 1(b). The holes occupy 12.4% of the total area. For fabrication, a co-polymer resist for electron-beam lithography was spin-coated on the glass substrate and the hole structures defined using electron beam lithography. A 2 nm Ti film and then a 40 nm Au film were deposited, followed by subsequent lift-off. This sample is typical of SPP-assisted EOT metallo-dielectric structures that have been studied to date.[3,5]

The optical setup consists of two synchronized mode-locked Ti:Sapphire oscillators with 82 MHz repetition rate, in which one laser delivers probe pulses at a wavelength of 770 nm (duration $\sim$1 ps) whereas the other is frequency-doubled to a wavelength of 415 nm (duration $\sim$200 fs) to serve as a source of pump pulses. Both the pump and probe polarizations are linear and are orientated perpendicular to each other and aligned along the symmetry directions of the lattice of square holes in the sample. The pump pulses are chopped at a frequency of 1 MHz using an acousto-optic modulator, and the time delay between each pump and probe pulse is scanned using a motorized mechanical stage. As shown in Fig. 1(a), the beams are combined with a dichroic mirror and are focused collinearly and at normal incidence on the sample surface using a $\times$10 microscope objective to a spot diameter of $\sim 5\,\mu$m (at full width at half maximum), encompassing approximately 40 holes in the sample. The energy of a single pump pulse is 40 pJ, which non-destructively leads to acoustic strains up to $\sim 10^{-4}$ in the sample through transient temperature rises of $\sim$30 K. The probe pulses have a similar energy. Because the acoustic excitation

a)Electronic mail: olly@eng.hokudai.ac.jp

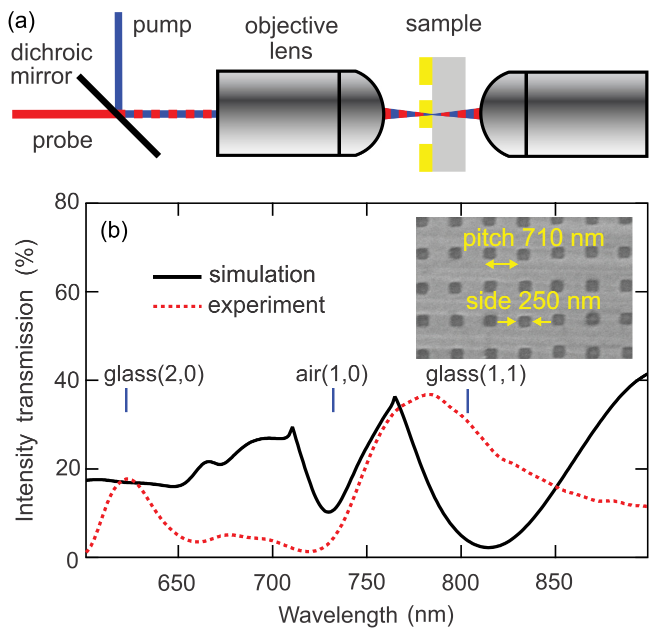

FIG. 1. (a) Schematic diagram of the pump-probe experiment. (Unit cell of the EOT structure is exaggerated.) (b) Experimental (red dashed line) and simulated (black solid line) optical transmission spectrum of the sample for normal incidence. The short vertical lines show the calculated positions of peaks (see text) characterized by integers (i, j) representing orders of in-plane Bragg-reflected SPPs for both the metal-air and metal-glass interfaces (marked air and glass, respectively). A SEM image of the sample is shown in the inset.

covers a large number of unit cells of the structure, only surface-phonon in-plane wave vectors $\mathbf{k}$ near the phononic Brillouin-zone center $\mathbf{k} = 0$ are excited, simplifying the spectrum of excited vibrational modes. The transmitted probe beam is directed to a photodiode connected to a lock-in amplifier referenced to the pump modulation frequency. An optical transmission spectrum was also recorded for normal incidence using a similar detection geometry with a white-light laser.

The measured optical transmission spectrum with incident unpolarized light is shown by the red dashed line in Fig. 1(b), exhibiting two principal maxima over the measured range. The simulated transmission spectrum for incident linear optical polarization aligned along the symmetry directions of the lattice of square holes, as shown by the black solid curve in Fig. 1(b), was calculated using COMSOL Multiphysics, assuming periodic boundary conditions and literature values of the refractive indices of the substrate and the 40 nm gold film.[11,12] (Because of the fourfold rotational symmetry of the sample structure, the transmission spectrum is independent of the in-plane orientation of the normally-incident linear polarization.) This spectrum also exhibits a main maximum near 780 nm, but the maxima clearly seen around 660–710 nm are very much smaller in experiment. These differences may be caused by the nanoscale roughness of the actual sample, deviations from ideal periodicity, or the finite numerical aperture (NA = 0.4) of the collection lens. In particular, for short wavelengths below the pitch of 710 nm, diffracted light exiting the sample at high angles to the normal is not collected, resulting in a lower transmission than in the simulation. The resonant enhancement of the main peak in the experiment is similar to that in the simulation, and the calculated strong transmission dip at $\sim$730 nm is also experimentally observed.[2] The basic shape of the spectrum, dependent on the in-plane plasmonic dispersion of the SPP crystal, is similar to those previously reported for square-hole EOT samples.[13] At normal incidence, one can identify characteristic resonant wavelengths λ_0 using an empty-lattice model of the plasmonic dispersion by solving the Equation[14,15]

$$(i^2 + j^2)^{1/2}\lambda_0 = a\mathrm{Re}\sqrt{\frac{\epsilon_1\epsilon_2(\lambda_0)}{\epsilon_1 + \epsilon_2(\lambda_0)}}, \tag{1}$$

where a is the lattice constant of the SPP crystal, ϵ_1 is the dielectric constant of the medium in contact with the metal (either air or glass in our case), and ϵ_2 is that of the metal. The integers i and j represent the orders of in-plane Bragg-reflected SPPs. From a knowledge of the dielectric constants of the gold film and substrate,[11,12] we find maxima in optical transmission corresponding to $(i, j) = (1, 0)$ for the metal-air interface, and (1,1) as well as (2,0) for the metal-glass interface, as indicated by the positions marked by short vertical lines in Fig. 1(b). (Because a large number of unit cells are simultaneously optically illuminated, only optical wave vectors near the center of the plasmonic Brillouin zone are excited.) These predictions are expected to lie on the shorter wavelength side of the actual peaks owing to the role of Fano processes.[16,17] This leads us to conclude that the main peak in transmission near 780 nm in both the experiment and simulation can be associated with the $(i, j) = (1, 0)$ resonance for the metal-air interface. The sharp feature observed at 710 nm in the simulation corresponds to the wavelength $(\lambda = a)$ expected for Wood's anomaly.[18] Its absence in the experiment is probably caused by spectral broadening arising from the use of a focused white light beam (to a spot size of $\sim 5\ \mu$m in diameter) — instead of a perfect normally-incident plane wave — or by imperfections in the sample.

Using literature values of the refractive index $n + ik = 0.174 + 4.79i$ of gold and for the glass substrate $n = 1.52$ (Ref. 11) at the pulsed probe wavelength of 770 nm,[12] we estimate the optical transmission based solely on a simple consideration of the relative area of the holes at this wavelength to be 15%. The simulated and experimentally measured transmissions are 31.1% and 34.5%, respectively, these two values being in relatively good agreement. Therefore, the effective transmission efficiencies for optical intensity are 2.1 and 2.3, respectively. These values are well above the threshold of 1 for extraordinary transmission. (In comparison, a uniform gold film of thickness of 40 nm on the same substrate would have a transmission of 4.2% at 770 nm.) The probe wavelength of 770 nm in the ultrafast experiments was chosen at an accessible point on the experimental optical transmission spectrum where there is a non-negligible gradient $dT/d\lambda$, where λ is the optical probe wavelength and T is the intensity transmission coefficient.

The experimental temporal variation of the relative transmission $\delta T(t)/T$ is shown in Fig. 2(a). Upon optical excitation, $\delta T/T$ shows a near-instantaneous reduction due to heating of the gold film. Subsequently, a complex pattern of oscillations is recorded. After subtracting the exponentially decaying thermal background, a temporal Fourier transform

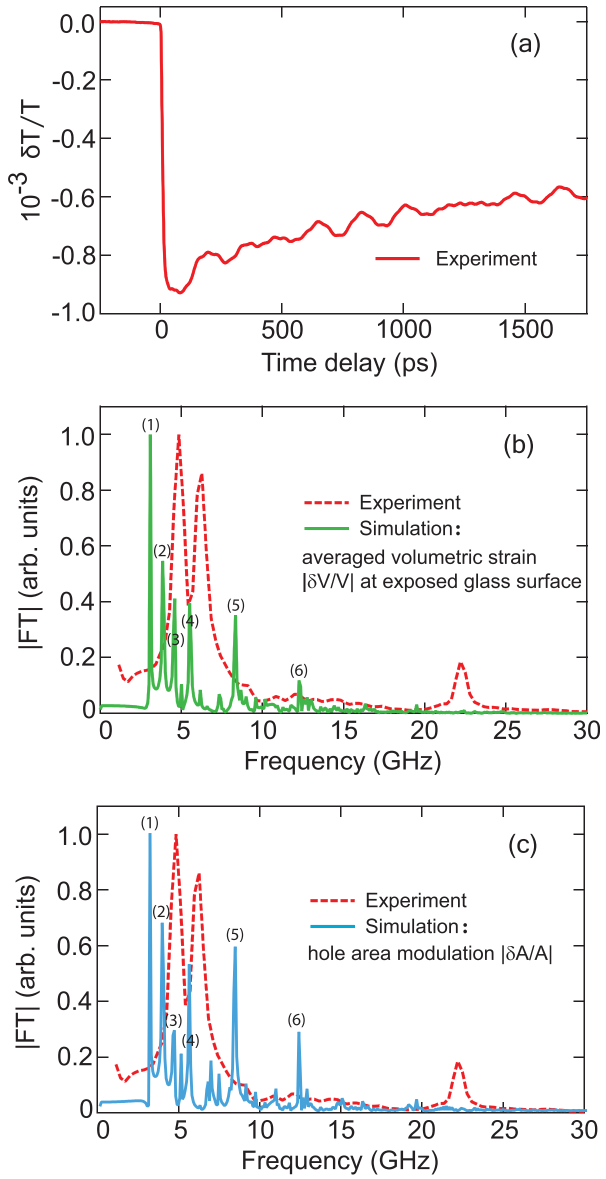

FIG. 2. (a) Experimental pump-induced transmission change of the sample as a function of the pump-probe delay, (b) corresponding magnitudes of the temporal Fourier transform (|FT|) of the experimental data (red dashed line) and simulation of the volumetric strain averaged over the exposed glass surface (green solid line), and (c) |FT| of the experimental data (red dashed line) and simulation of the relative hole-area modulation (blue solid line).

(FT), the magnitude of which is shown by the red dashed graph in Fig. 2(b), reveals two main resonances at 5 and 6.5 GHz, a smaller one at 9 GHz, and several even smaller features above 10 GHz. The peak at 22 GHz is caused by Brillouin scattering of the propagating longitudinal strain pulse in the glass substrate;[19–22] the predicted frequency is given by $f_B = 2nv_l/\lambda$, where λ is the optical probe wavelength, n is the refractive index of the glass substrate, and v_l is the longitudinal sound velocity in glass. Using reasonable estimates of $n = 1.52$ and $v_l = 5710$ m/s,[11] we find the predicted $f_B = 22.5$ GHz, in good agreement with experiment.

In order to understand the origin of this vibrational spectrum, we performed numerical simulations. Transient deformations in the structure (apart from the ultrathin Ti film that was neglected) were calculated using PZFlex software (Weidlinger Associates, Inc.), using a mesh size of 4 nm, a time step of 0.52 ps, and a total simulation time of 12 ns. The unit cell of 710 nm × 710 nm × 80 μm containing a single hole is modeled with symmetric boundary conditions (BCs) in the lateral directions to effectively reduce the sample volume (and render the analysis equivalent to periodic BCs in the lateral directions). Absorbing BCs were used on the other surfaces, with the top surface remaining free. (The substrate thickness was reduced from 1 mm to 80 μm to economize on calculation time.) A downward vertical force field in the form of a half sine wave of duration 50 ps was applied uniformly over all the top gold surface, adequate to reproduce qualitatively the broadband GHz excitation in the experiment. The sound velocities and densities appropriate for gold and glass were assumed to be $v_l = 3240$ m/s, $v_t = 1200$ m/s, and $\rho = 19\,300$ kg/m^3 and $v_l = 5710$ m/s, $v_t = 3467$ m/s, and $\rho = 2510$ kg/m^3, respectively.[11,12,23] To obtain a measure of the spectrum of the modulated optical properties of the EOT structure, we plot in Fig. 2(b) by the solid green line the normalized modulus of the temporal FT of the averaged volumetric complex strain amplitude $|\delta V/V|$ over the top surface of the exposed regions of the glass substrate, i.e., in the regions of the holes. Several sharp resonances are evident, corresponding to individual surface-confined vibrational modes of the sample. In particular, 6 main resonances are detected at 3.1, 3.8, 4.6, 5.5, 8.3, and 12.3 GHz. These frequencies lie in the same overall frequency region as the three main experimental peaks, but do not correspond exactly. As a detailed theory of the modulation of the electromagnetic fields by the deformed sample is beyond the scope of this work, we are not able to make a more precise prediction of the amplitudes of the observed experimental peaks. However, it is clear that the photoelastic effect from the strain in the exposed regions of glass[24] (i.e., the holes) and the direct modulating effect of the deformed contour of the holes should both contribute to the modulation in transmission.[25,26] In this connection, it is interesting to also compare the experimental spectrum of $\delta T/T$ with that for the relative modulation of the area of the holes: the solid blue line in Fig. 2(c) is the normalized modulus of the maximum relative area change of the holes at a particular frequency, $|\delta A/A|$, obtained by sampling a series of images of the real part of the temporal FT at each frequency (see below for animations). The spectrum for $|\delta A/A|$ is similar to that for $|\delta V/V|$, with the same 6 resonant frequencies being dominant, but their relative amplitudes are somewhat different. As observed in the experiment, the lowest frequencies appear with enhanced amplitude. Although not considered here, the light leaking through the gold film may also contribute to the modulation because of the photoelastic effect in the underlying glass. (At the probe wavelength, we expect the photoelastic effect in gold to be negligible.[27]) The observed resonant widths of the experimental peaks appear to be greater than those predicted by the simulation, possibly owing to inhomogeneous broadening caused by hole roughness or hole-pitch variations. This could also be the cause of the slight differences in the experimental resonant frequencies compared to those simulated. As for the relative heights of the peaks, these are not expected to follow those in the experiment because of the neglect in the acoustic simulations of all aspects of the optical response. However, we can partially elucidate the origin of the transmission modulation by examining the absolute ratio $|\delta A/A|/|\delta V/V|$ found

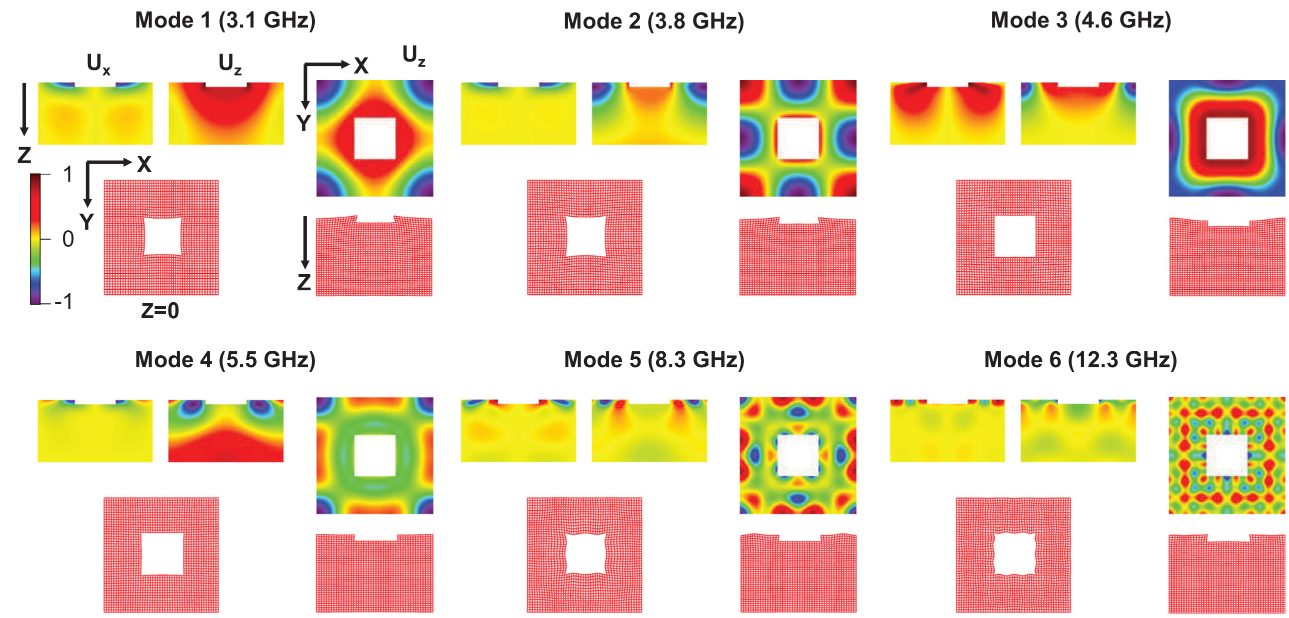

FIG. 3. Deformation fields of the simulated vibrational modes at 6 resonant frequencies, calculated from the real part of temporal Fourier transforms at each point. x and y are the in-plane coordinates, whereas z is the out-of-plane coordinate. The amplitudes are greatly exaggerated in the mesh images. Animations can be viewed in the supplementary material.

in the acoustic simulation at the six principal acoustic resonant frequencies: we obtain 2.9, 3.2, 2.1, 3.3, 4.9, and 5.7, respectively, for this ratio. Owing to the relatively small values of the photoelastic constants ($p_{12} = 0.27$ and $p_{11} = 0.12$) in glass,[24] it is therefore likely that the hole-area modulation provides the dominant transmission-modulation mechanism in our sample.

To see the effect of the acoustic vibrations on the structure more clearly, we plot for each of the 6 main simulated resonances the form of the sample deformation as well as cross sections of the displacement fields in Fig. 3. It is evident from these plots that the hole shape is modulated by the oscillating strain. Animations of the hole motion can be viewed elsewhere (see supplementary material), showing that all 6 resonances involve a variation in $\delta A/A$.

To further understand the origin of these simulated vibrational modes, we maintained the hole size and shape constant while varying the hole pitch a, i.e., the lattice constant, over the range $a = 710 \pm 80$ nm. The frequencies were all found to depend on a, as shown in Fig. 4(a). The dependences can be better understood by the plot against $1/a$ in Fig. 4(b). The dashed lines in this figure are fits $\propto 1/a$. This behavior is commonly observed in other phononic crystal structures[28,29] and indicates the presence of collective vibrational modes with surface phononic wave vectors near $\mathbf{k} = 0$, as previously mentioned, rather than isolated modes inside a single unit cell.

In conclusion, using femtosecond transient absorption spectroscopy in the near-infrared, we have measured the ultrafast optical response associated with the GHz acoustic modulation of an EOT geometry using a metamaterial consisting of a thin gold film patterned with a regular array of sub-optical-wavelength size square holes. Several collective vibrational modes of the array in the frequency range ~3 to 12 GHz were clearly identified to be photoexcited by the optical pump pulses and to give rise to a modulation in transmission δT. Simulations of the transient deformations of the sample give reasonable overall agreement with the resonant frequencies observed in the experiment and suggest that both the strain in the exposed glass regions and the modulation of the relative area of the holes can contribute to δT. A comparison of the hole-area modulation and the strain

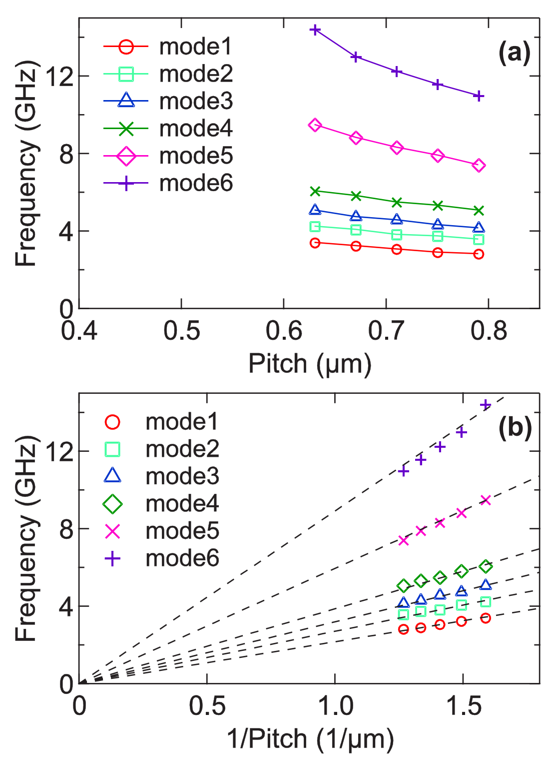

FIG. 4. (a) Plot of the 6 main simulated resonant frequencies of the sample vs hole pitch a for a constant hole size. The solid lines are a guide to the eye. (b) Plot against $1/a$. The straight dashed lines in (b) are fits in the form $f = K/a$, where f is the mode frequency and K is an adjustable constant.

amplitude in the glass substrate in the hole regions suggests that the hole-area modulation provides the dominant transmission-modulation mechanism in our sample. Many more experiments await trial in this field. For example, it would be interesting to determine how the acoustic modulation affects the optical emission patterns from EOT structures or determine whether acoustically induced changes in surface topography can contribute to the EOT modulation. Moreover, by tailoring the properties of the regular array of nano-holes and their plasmonic dispersion, it may be possible to design structures with an enhanced acousto-optic interaction, thereby opening up the arena of efficient ultrafast acoustic modulation using extraordinary optical transmission.

See supplementary material for animations of the motion of a unit cell of the EOT structure shown in top and side views at 6 resonant frequencies.

[1] R. Ulrich, in *Symposium on Optical and Acoustical Micro-Electronics* (1975), Vol. 1, pp. 359–376.
[2] T. W. Ebbesen, H. Lezec, H. Ghaemi, T. Thio, and P. Wolff, Nature **391**, 667 (1998).
[3] C. Genet and T. Ebbesen, Nature **445**, 39 (2007).
[4] P. Lalanne, J.-P. Hugonin, H. Liu, and B. Wang, Surf. Sci. Rep. **64**, 453 (2009).
[5] S. Collin, Rep. Prog. Phys. **77**, 126402 (2014).
[6] H.-T. Chen, H. Lu, A. K. Azad, R. D. Averitt, A. C. Gossard, S. A. Trugman, J. F. O'Hara, and A. J. Taylor, Opt. Express **16**, 7641 (2008).
[7] W. Gao, J. Shu, K. Reichel, D. V. Nickel, X. He, G. Shi, R. Vajtai, P. M. Ajayan, J. Kono, D. M. Mittleman *et al*., Nano Lett. **14**, 1242 (2014).
[8] L. L. Guyader, A. Kirilyuk, T. Rasing, G. Wurtz, A. Zayats, P. Alkemade, and I. Smolyaninov, J. Phys. D: Appl. Phys. **41**, 195102 (2008).
[9] D. Gérard, V. Laude, B. Sadani, A. Khelif, D. Van Labeke, and B. Guizal, Phys. Rev. B **76**, 235427 (2007).
[10] S.-C. Yang, H.-P. Chen, H.-H. Hsiao, P.-K. Wei, H.-C. Chang, and C.-K. Sun, Opt. Express **20**, 16186 (2012).
[11] See http://www.schott.com/advanced_optics/english/syn/advanced_optics/products/optical-materials/thin-glass/thin-glass-d-263-t-eco/index.html for the physical properties of glass substrate.
[12] *Handbook of Optical Constants of Solids*, edited by E. D. Palik (Academic Press, Boston, 1998).
[13] K. Van der Molen, K. K. Koerkamp, S. Enoch, F. Segerink, N. Van Hulst, and L. Kuipers, Phys. Rev. B **72**, 045421 (2005).
[14] H. Ghaemi, T. Thio, D. Grupp, T. W. Ebbesen, and H. Lezec, Phys. Rev. B **58**, 6779 (1998).
[15] W. Dickson, G. A. Wurtz, P. R. Evans, R. J. Pollard, and A. V. Zayats, Nano Lett. **8**, 281 (2008).
[16] C. Genet, M. van Exter, and J. Woerdman, Opt. Commun. **225**, 331 (2003).
[17] M. Sarrazin, J.-P. Vigneron, and J.-M. Vigoureux, Phys. Rev. B **67**, 085415 (2003).
[18] D. Maystre, *Plasmonics* (Springer, 2012), pp. 39–83.
[19] O. Matsuda, M. C. Larciprete, R. L. Voti, and O. B. Wright, Ultrasonics **56**, 3 (2015).
[20] H.-N. Lin, H. Maris, L. Freund, K. Lee, H. Luhn, and D. Kern, J. Appl. Phys. **73**, 37 (1993).
[21] A. M. Lomonosov, A. Ayouch, P. Ruello, G. Vaudel, M. R. Baklanov, P. Verdonck, L. Zhao, and V. E. Gusev, ACS Nano **6**, 1410 (2012).
[22] T. Dehoux, K. Ishikawa, P. H. Otsuka, M. Tomoda, O. Matsuda, M. Fujiwara, S. Takeuchi, I. A. Veres, V. E. Gusev, and O. B. Wright, Light: Sci. Appl. **5**, e16082 (2016).
[23] *CRC Handbook of Chemistry and Physics*, 85th ed., edited by D. R. Lide (CRC Press, Boca Raton, FL, 2004).
[24] R. Dixon, J. Appl. Phys. **38**, 5149 (1967).
[25] T. Kelf, Y. Tanaka, O. Matsuda, E. Larsson, D. S. Sutherland, and O. Wright, Nano Lett. **11**, 3893 (2011).
[26] T. A. Kelf, W. Hoshii, P. H. Otsuka, H. Sakuma, I. A. Veres, R. M. Cole, S. Mahajan, J. J. Baumberg, M. Tomoda, O. Matsuda, and W. O. B, New J. Phys. **15**, 023013 (2013).
[27] M. Garfinkel, J. Tiemann, and W. Engeler, Phys. Rev. **148**, 695 (1966).
[28] H. Sakuma, M. Tomoda, P. H. Otsuka, O. Matsuda, O. B. Wright, T. Fukui, K. Tomioka, and I. A. Veres, Appl. Phys. Lett. **100**, 131902 (2012).
[29] J.-F. Robillard, A. Devos, I. Roch-Jeune, and P. Mante, Phys. Rev. B **78**, 064302 (2008).